Self-Assembly of AB Diblock Copolymers under Confinement into Topographically Patterned Surfaces

Guang Yang,[†,‡] Ping Tang,*[,†,‡] Yuliang Yang,[†,‡] and Joao T. Cabral[†,§]

Key Laboratory of Molecular Engineering of Polymers of Ministry of Education and Department of Macromolecular Science, Fudan University, Shanghai 200433, China, and Department of Chemical Engineering, Imperial College, London SW7 2BY, U.K.

Received: April 11, 2009; Revised Manuscript Received: August 18, 2009

Motivated by recent experiments of copolymer patterning by nanoimprinting, we investigate microphase separation and morphology for symmetric AB diblock copolymers with lamellar structure in bulk, confined between a flat bottom surface and a square-wave top surface by using the self-consistent field theory (SCFT). The efficient and high-order accurate pseudospectral method is adopted to numerically solve the SCFT equations in irregularly shaped domains with the help of the "masking" technique by embedding the confined domains of arbitrary shape within a larger rectangular computational cell. Our simulations reveal that the inverted T-style and trapezoid structures occurring in the relatively strong and weak surface fields, respectively, are following our topographically patterned surface. For neutral walls, when the thickness of the lower section is commensurate with the lamellae period of bulk block copolymers, the topographically patterned surface in this work leads to parallel lamellae, and completely parallel lamellae are favored when both the width and height of the upper section are equal to the lamellae bulk period. Furthermore, the prevalent structures are the parallel lamellae in the upper section combined with the perpendicular lamellae in the lower section. When the walls repel one of the block species, parallel lamellae occur in a wide range of film thicknesses compared to the case of neutral walls. To our knowledge, some new structures, however, such as square and partial square structures and reversed-T and trapezoid structures, have not been reported before under parallel surface confinement. In general, the required structures can be obtained by choosing the proper degree of spatial confinement, characterized by variations of the ratio of film thicknesses to bulk repeat period, and the block−substrate interactions. Moreover, we show that the confinement width of the lower section (or the period of the square wave) plays a critical role in microstructure formation. These findings provide a guide to designing novel microstructures involving symmetric diblock copolymers via topographically patterned surfaces and surface fields, relevant to nanoimprinting.

Introduction

Diblock copolymers are composed of two distinct polymer chains joined chemically at their ends to prevent macrophase separation of different species, which can self-assemble into a variety of nanoscale morphologies such as lamellae (LAM), hexagonally packed cylinders (HEX), and body-centered cubic (BCC) spheres and more complex structures such as gyroids (G) in melts and solutions.[1,2] This microphase separation has therefore attracted considerable attention in the area of soft condensed matter physics and nanotechnology.[3,4] Frequently, however, the orientation of the nanodomains is imperfect or the grain size is small for practical applications such as in photonics or data storage. Therefore, block copolymers confined to physically or chemistry defined patterns have been proposed to control orientation and long-range ordering of the domains.[5] In bulk, the morphology of block copolymers is determined mainly by the molecular architecture and the interaction between the different components.[2] However, thin film confinement has a great influence on the phase behavior of block copolymers,[6−8] and controlling the microdomain ordering in thin films has thus attracted much attention for applications in polymer optical lithography.[9−13] In comparison to the phase structure in bulk, two effects emerge in confinement. On the one hand, the commensurability of the natural microdomain spacing in bulk with the film thickness can impact the alignment of the structure; on the other hand, the interactions between the block species and the surface (the surface field) may cause the surface segregation. By tuning the geometric confinement and the interactions between polymers and surfaces, large scale alignment of a surface reconstruction and a series of complex morphologies can be obtained in thin films.[14−16]

Many studies have centered on the control of the morphology of diblock copolymer systems under various confinements such as thin films,[14,15,17−23] cylindrical pores,[24−26] hexagonal walls,[27] spheres,[28,29] thin films on corrugated substrates,[30−32] and systems that involve the inclusion of filler particles,[33] or nanorods.[34] Recently, chemical prepatterning[11,35−37] and graphoepitaxy[12] techniques are used to direct translational ordering and feature registration of block copolymers. However, the experimental techniques involved in patterning substrates with chemical or physical features on the same length scale as the blocks require sophisticated and costly processing.[38] In this regard, computer simulations provide a convenient and effective role in guiding the experiments. Up to now, a few theoretical studies[31,32] have been conducted on the self-assembly of block copolymer

* Corresponding author. E-mail: pingtang@fudan.edu.cn.
† Key Laboratory of Molecular Engineering of Polymers of Ministry of Education, Fudan University.
‡ Department of Macromolecular Science, Fudan University.
§ Imperial College.

10.1021/jp9033613 CCC: $40.75
Published on Web 10/08/2009

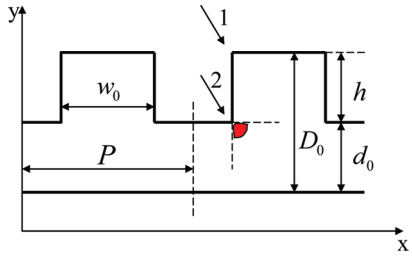

Figure 1. Schematic description of the confinement geometry of diblock copolymers with a flat bottom and square-wave top surfaces (two periodical confined units shown here). The alternative convex and concave thicknesses along the y direction are D_0 and d_0, respectively. The height of the upper section is h. The width of the lower section (or the period of the square wave) is P, and the width of the upper section is w_0 along the x direction.

confined films in which one surface is topographically patterned and another one is flat. Podariu[31] investigated the phase behavior of block copolymer thin films on a physically corrugated substrate with the phenomenal TDGL model. The relative stability of parallel and perpendicular lamellar layers on corrugated surfaces was considered on the theoretical modeling.[32] In this work, we use self-consistent field theory to systematically evaluate the phase behavior of a system of symmetric diblock copolymers confined between horizontal asymmetrical surfaces, of which the lower surface is flat and the upper surface is a square wave, as shown in Figure 1. In fact, this film model is analogous to the experimental report by Kim et al.[39] and relevant to nanoimprinting of block copolymers. Quite recently, Park et al.[40] studied block copolymers supported by a rigid square-wave (bottom) substrate, but the top layer of the film was a free surface in contact with air. This is very different from our simulations considered in this work. However, we both found that the alignment of lamellae is strongly dependent on the relative film thickness to corrugation depth as well as the period of the surface corrugation.

Thin films of symmetric AB diblock copolymers are the simplest confined systems and have been extensively studied in simulations[19,41−44] and theories.[7,14,18,45−48] Shull et al.[45] used self-consistent field theory (SCFT) to probe whether the period of lamellae layers increased or decreased to accommodate the different thicknesses of thin films. Turner[7] noticed that the configurations with an odd-integer number of layers occurred only when the difference between the two polymer−plate surface tensions was small, and only below some critical plate separation. Monte Carlo simulations (MC) by Kikuchi and Binder[46] showed that not only the period of lamellae but also the orientation of the layers changed with different film thicknesses. Further, Matsen[18] investigated substrates with different interactions with the copolymers and systematically computed the phase behavior of symmetric diblock copolymers confined in films with various conditions. In 1999, Geisinger[42,43] et al. used SCFT and Monte Carlo simulations confirming the results obtained by Matsen. The phase behavior of confined symmetric diblock copolymers is reasonably well understood. When the substrates are neutral to both species, the lamellae phase perpendicular to the substrates is always stable. However, when the substrates have a preference of one species, the microphases alternate between parallel and perpendicular lamellae as the thickness of the thin film increases. SCFT has proved to be one of the most successful theoretical methods for investigating equilibrium phases in block copolymers and has played a major role in establishing the phase diagram of bulk block copolymer melts.[49,50] Matsen[18] first applied the SCFT of Helfand[51] to thin films of symmetric AB diblock copolymers, and assumed that the total segment density rises continuously from zero to the bulk value following a cosine function within a distance (interface) from each wall based on the assumption that the total segment density would vanish on the confining walls. Wang et al.[52] evaluated the profiles at the interface using different functional forms and revealed that the choice of the profile strongly influences the numerical performance of the SCFT calculations. Fredrickson et al.[27,53] adopted a simple "masking" technique that confines the block copolymer between two walls by choosing a "masking" function to fit the geometry of the film. In our work, Fredrickson's masking trick is borrowed similarly to deal with the complicated geometrical confinement effect of block copolymers. In particular, the pseudospectral method is used to numerically implement the SCFT equations in irregularly shaped domains. We focus on a typical symmetric composition ($f_A = 0.5$, where f_A is the volume fraction of the A block) diblock copolymer and assume that the two confining substrates have the same selectivity to the copolymers (symmetric wetting or dewetting). The confinement effect on the phase behavior of the system is thus systematically investigated as a function of film geometry (the parameters of D_0, d_0, h, P, and w_0 denoted in Figure 1) and surface field strength.

Recently, He et al.[54] reported the phase behavior of diblock copolymers with the volume fraction $f = 0.4$ confined in asymmetric topographies with the upper flat and lower square-wave substrates. Compared to their study, we systematically study the effects of the confinement geometry and surface field on the pattern formation of block copolymers with symmetric composition $f = 0.5$. Moreover, we discuss the effect of important parameters of the width of the upper section w_0 and the lower section P, i.e., the period of the square wave in this complex confined geometry, which is found to be significant in inducing additional complicated morphologies in this work. We build upon the "masking" technique proposed by Fredrickson et al.[27,53] to include a hyperbolic tangent profile that minimizes the number of Fourier modes required to resolve the wall region while retaining the stability characteristics of standard saddle point search methods. Last but not least, compared to the real-space solution of the diffusion equation of chain propagators, the pseudospectral method involving fast Fourier transforms (FFTs) originally proposed by Rasmussen et al.[55] is more efficient and accurate.

Theoretical Model

In this section, we briefly describe the SCFT simulation method employed to predict the equilibrium structure of AB diblock copolymers confined between two horizontal asymmetrical surfaces, as shown in Figure 1. The alternative convex and concave thicknesses along the y direction are D_0 and d_0, respectively. The height of the upper section is h (i.e., $h = D_0 - d_0$). The width of the lower section (or the period of the square wave) is P, and the width of the upper section is w_0 along the x direction. Although the system is not completely confined along the x direction, the period of the square wave P determines the shape of the confinement geometry, thus significantly influencing the morphologies of diblock copolymers. We consider a melt of an AB diblock copolymer melt occupying volume V. Each polymer has the same chain length N with A block volume fraction f_A. The bulk monomer density ρ is assumed to be the same for all chemical species. We scale distances by the Gaussian radius of gyration: $R_g = a(N/6)^{1/2}$, where a is the monomer statistical Kuhn length. We follow the "masking" technique proposed by Fredrickson et al.[27,53] and

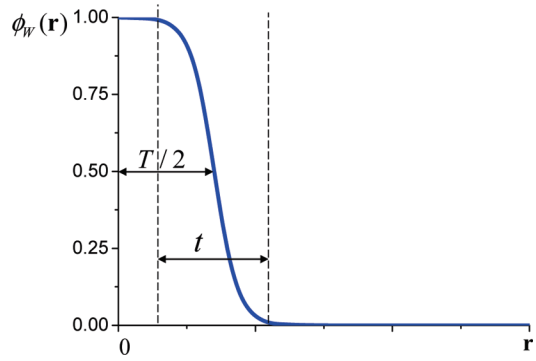

Figure 2. Surface density field $\phi_W(\mathbf{r})$ corresponding to eq 1 showing the depth profile of the interfacial density field, as a function of distance $\mathbf{r}$ from the wall surface. Here, $T = 0.5R_g$ and $t = 0.25R_g$.

adopted later in our previous publication[56] to realize the confinement geometry of block copolymers. The main idea of this method is that a surface density field, $\phi_W(\mathbf{r})$ (here, W stands for wall, $0 \le \phi_W(\mathbf{r}) \le 1$), is introduced to confine the polymers into the enclosed region by the wall surfaces; $\phi_W(\mathbf{r}) = 0$ in the polymer area, while $\phi_W(\mathbf{r}) = 1$ out of the polymer area. The polymers are expelled by imposing an incompressibility constraint, namely, $\phi_A(\mathbf{r}) + \phi_B(\mathbf{r}) + \phi_W(\mathbf{r}) = 1$. Therefore, the choice of $\phi_W(\mathbf{r})$ determines the geometry of the films and here the transition is selected to be a hyperbolic tangent functional form:

$$\phi_W(\mathbf{r}) = \frac{1}{2}\left\{1 - \tanh\left[\frac{m}{t}\left(d_\perp(\mathbf{r}) - \frac{T}{2}\right)\right]\right\} \quad (1)$$

Equation 1 is sketched in Figure 2, which describes a planar cavity field with an overall "cavity thickness"[53,56] T to represent the range of wall interactions along position $\mathbf{r}$. Here, m and t are factors used to define the transition region and to set the width of the transition region, respectively; $d_\perp(\mathbf{r})$ is the distance from the position $\mathbf{r}$ to the nearest edge of the boundary of the wall. The boundary of the wall is the outmost point of the cavity thickness (i.e., where $\phi_W(\mathbf{r}) \approx 1$). In this way, it is easy to compute $d_\perp(\mathbf{r})$ along most of the walls including arrow 1 shown in Figure 1, but obviously, we have to find another way to deal with the positions of walls indicated by arrow 2 and the corresponding red region of the figure. In this case, $d_\perp(\mathbf{r})$ is defined as the distance from the point $\mathbf{r}$ to the crossing point (indicated by arrow 2) of two walls; t is the interfacial thickness of the transition from wall to polymers, and the interface becomes sharper with decreasing t or increasing m, which is suitable for describing a small interfacial thickness. The value of m should be chosen as $4 \le m \le 6$ to ensure that the value of tanh() can infinitely approach values of 1 and -1, as a function of film thickness. In this work, the value of m is chosen as $m = \ln(99) \approx 4.60$ so that the wall transition region is defined to begin at $\phi_W(\mathbf{r}) = 0.99$ and end at $\phi_W(\mathbf{r}) = 0.01$. On the one hand, values of T should be chosen larger than the transition thickness t to prevent the overlap of the interfaces; on the other hand, we do not expect the specific value of T to affect the results; therefore, T should be selected smaller than R_g (i.e., $T \approx 0.5R_g$ in this work). In fact, a suitable narrow and smooth transition region between $\phi_W(\mathbf{r}) = 0$ in the interior and $\phi_W(\mathbf{r}) = 1$ in the exterior of the confinement determines the accuracy of this method in complex irregular domains. We tested that for the same T the number of points that lie in the interface (with the number of points varying in this case from 4 to 8 points) assures the space discretization accuracy for confined geometry. Thus, the effective thicknesses of the confinement system should be $D = D_0 - T$, $d = d_0 - T$, and $w = w_0 - T$, respectively. We should note that the "masking" function adopted by us is similar to that used by Matsen,[18] differing only in functional form, namely, the cosine. In this paper, we opt for a hyperbolic tangent function to minimize the number of lattice points needed to resolve the region $(0 < \phi_W(\mathbf{r}) < 1)$ for the required Fourier modes as the cosine function need much more lattice points to obtain, such as the same cavity thickness T, in comparison.[27] Also, the hyperbolic tangent function retains the stability characteristics of standard saddle point search methods. Furthermore, the confining wall is modeled as a fixed density field that interacts with the polymer segments via the incompressibility constraint and Flory−Huggins interactions.

In the SCFT model, one considers the statistics of a single copolymer chain in a set of effective chemical potential fields $\omega_i(\mathbf{r})$, where i represents block species A and B. The free energy per chain may be calculated as

$$\frac{F}{nk_BT} = -\ln\left(\frac{Q}{V}\right) + \frac{1}{V}\int d\mathbf{r}\chi_{AB}N\phi_A\phi_B + \frac{1}{V}\int d\mathbf{r}(\chi_{AW}N\phi_A\phi_W + \chi_{BW}N\phi_B\phi_W) - \frac{1}{V}\int d\mathbf{r}(\omega_A\phi_A + \omega_B\phi_B) - \frac{1}{V}\int d\mathbf{r}\xi(1 - \phi_A - \phi_B - \phi_W) \quad (2)$$

where χ_{AB} is the Flory−Huggins interaction parameter between different species A and B and χ_{iW} is a dimensionless measure of the surface energy between species i and the walls. $\xi(\mathbf{r})$ is a relaxation parameter that ensures the incompressibility of the system, and V represents the effective volume occupied by copolymers: $V = \int d\mathbf{r}(1 - \phi_W(\mathbf{r}))$. $Q = \int d\mathbf{r}q(\mathbf{r}, s)q^+(\mathbf{r}, N - s)$ is the partition function of a single chain. The segment distribution function $q(\mathbf{r}, s)$ and $q^+(\mathbf{r}, s)$ for a single chain of contour length s at position $\mathbf{r}$ with inclusion of end segment can be obtained by the modified diffusion equations:[51]

$$\frac{\partial q(\mathbf{r}, s)}{\partial s} = \begin{cases} \frac{Na^2}{6}\nabla^2 q(\mathbf{r}, s) - \omega_A(\mathbf{r})q(\mathbf{r}, s) & \begin{pmatrix} q(\mathbf{r}, s): s \le Nf_A \\ q^+(\mathbf{r}, s): s \ge N - Nf_A \end{pmatrix} \\ \frac{Na^2}{6}\nabla^2 q(\mathbf{r}, s) - \omega_B(\mathbf{r})q(\mathbf{r}, s) & \begin{pmatrix} q(\mathbf{r}, s): s > Nf_A \\ q^+(\mathbf{r}, s): s < N - Nf_A \end{pmatrix} \end{cases} \quad (3)$$

with initial condition $q(\mathbf{r}, 0) = 1$. The other $q^+(\mathbf{r}, s)$ is expressed analogously to eq 3 with initial condition $q^+(\mathbf{r}, 0) = 1$. According to mean-field approximation, minimization of the free energy with respect to densities and chemical potentials leads to the following equations:

$$\phi_A(\mathbf{r}) = -V\frac{\delta \ln Q}{\delta \omega_A} = \frac{V}{NQ}\int_0^{f_AN} ds q(\mathbf{r}, s)q^+(\mathbf{r}, N - s) \quad (4)$$

$$\phi_B(\mathbf{r}) = -V\frac{\delta \ln Q}{\delta \omega_B} = \frac{V}{NQ}\int_{f_A N}^{N} ds q(\mathbf{r}, s) q^+(\mathbf{r}, N-s) \quad (5)$$

$$\omega_A(\mathbf{r}) = \chi_{AB} N \phi_B(\mathbf{r}) + \chi_{AW} N \phi_W(\mathbf{r}) + \xi(\mathbf{r}) \quad (6)$$

$$\omega_B(\mathbf{r}) = \chi_{AB} N \phi_A(\mathbf{r}) + \chi_{BW} N \phi_W(\mathbf{r}) + \xi(\mathbf{r}) \quad (7)$$

$$\phi_A(\mathbf{r}) + \phi_B(\mathbf{r}) + \phi_W(\mathbf{r}) = 1 \quad (8)$$

where $\phi_A(\mathbf{r})$ and $\phi_B(\mathbf{r})$ are the average densities of A and B segments at $\mathbf{r}$. Equations 3−8 form a closed set of self-consistent equations. The equations are numerically implemented by the combinatorial screening algorithm proposed by Drolet and Fredrickson.[49,50] First, random initial values of field $\omega_i(\mathbf{r})$ are given. Second, the diffusion equation (eq 3) is solved to obtain $q(\mathbf{r}, s)$ and $q^+(\mathbf{r}, s)$ with the pseudospectral numerical method.[55] Third, the density fields are evaluated by eqs 4 and 5. Finally, with the obtained segment density, the fields $\omega_i(\mathbf{r})$ and $\xi(\mathbf{r})$ are updated by a combination of their old and new values according to eqs 6−8. With the new fields, the partition functions $q(\mathbf{r}, s)$ and $q^+(\mathbf{r}, s)$ are evaluated again to obtain the segment density. These steps are iterated until the free energy converges to a stable value, the change at each iteration is reduced to 10^{-5}, and the phase pattern emerging in the simulation box can be clearly identified.

The simulations are carried out on a two-dimensional space with $L_x \times L_y$ lattice, in which we constrain the densities out of the template $\phi_W(\mathbf{r}) = 1$ to satisfy periodic boundary conditions in the x and y directions both in bulk and in confinement. The discretization of the parameters is chosen to be $\Delta s = 1/100 = 0.01$; namely, the contour length is discretized into 100 segments. The grid size is $\Delta x = \Delta y = 0.0625 R_g$ to ensure a fine spatial resolution for relatively narrow transitions between interior and exterior areas of polymers. We test the reliability of this discretization in the second-order pseudospectral method and confirm that the morphologies are accurate, i.e., the convergence of the free energy and chemical potential are almost unchanged compared with $\Delta x = \Delta y < 0.0625 R_g$. Furthermore, the final stable structure is determined by comparing the minimization of the free energy repeated at least three times by using different random initial states of fields $\omega_i(\mathbf{r})$ and different random numbers to guarantee that the structure is not occasionally observed.

Results and Discussion

The confined AB diblock copolymer film is specified by the follow parameters: f_A, $\chi_{AB}N$, $\chi_{iW}N$, and geometrical confined shape parameters such as D, h, d, P, and w. For the sake of simplicity, in our simulation, we fix $f_A = 0.5$, namely, symmetric diblock copolymers, which is a representative volume fraction of a lamella phase in the bulk. The Flory−Huggins parameter between different species A and B is set as $\chi_{AB}N = 35$ corresponding to an intermediate degree of segregation. Due to the symmetry of A and B segments, we assume that the surface walls are neutral to species B ($\chi_{BW}N = 0$) but have interactions with the component A. $\chi_{AW}N > 0$ means a repellent effect for the segment A toward the surface, while $\chi_{AW}N < 0$ means surface attraction for segment A. The copolymer repeat period in the bulk L_0 is calculated to be $4.58 R_g$, and the overall cavity thickness is $T = 0.5 R_g \approx 0.11 L_0$. For simplicity, we fix a variety of w and D with the increment $0.5 L_0$, and set the ratio h/d_0 to be 1:1 and 2:1. For clarity and convenience describing the phase behavior in structured films, the topographic pattern is divided into two parts: (a) the upper section, having three confined surfaces around the width of w_0 and the height of upper section h, and (b) the lower section having two confined surfaces except the connecting region with the upper section, both of which join together and are affected by the convex confined thickness $D_0(D)$ and the period of the square wave P. Under different surface fields (weak and strong A-repellent surfaces), the self-assembled structures are investigated as a function of confinement dimensions w/L_0, P/L_0, h/L_0, d/L_0, and D/L_0.

A. For Neutral Walls. Both frustration effects by confinement and surface fields play important roles in polymer self-assembly in thin films. To distinguish them, we first consider AB diblock copolymers to be confined between neutral walls that do not interact with either polymer species ($\chi_{AW}N = \chi_{BW}N = 0$) in order to evaluate the effect of confinement alone. It is known that symmetric AB diblock copolymer forms mostly lamellar phases both in bulk[1,2] and in confinement.[18] By forming a lamella phase, the system minimizes the number of A−B contacts, thereby reducing the energy of interaction between unlike A−B monomers at the expense of corresponding polymer entropy due to the localization of monomers into domains.[7] Here, the symbol v denotes the number of A/B interfaces in the lamellar phase. Figure 3 shows the calculated phase diagrams corresponding to different values of confinement sizes including w/L_0, D/L_0, h/L_0, d/L_0, and P/L_0 for the case of neutral walls. Two different colors, red and green, are assigned to A and B blocks, respectively. For clarity, the column numbers and row letters are used to denote the structures in the diagram. In the spatial confinement we have explored, these microstructures are divided into three primary classes in terms of phase behavior. The first one is the mix of parallel and perpendicular alignments of lamellae. The lamellae are parallel to the top surface of the upper section and perpendicular to the bottom substrate, including most microstructures shown in the condition of $w/L_0 = 0.43$ ($w_0/L_0 = 0.53$) and structures in L2, M2, N2, M3, N3, J4, M4, and N4 for the case of $w/L_0 = 0.86$ ($w_0/L_0 = 0.96$). It should be noted that the first class structures are commonly found when the height of upper section h is larger than or equal to w, especially for $d < L_0$. The second class is that all the lamellae are completely perpendicular to both of the top and bottom surfaces, as shown for the case of $w/L_0 = 0.86$, $D/L_0 = 0.96$, or $h \approx d \approx 0.5 L_0$ (i.e., $w \approx L_0$ and $h < w$, in column 1), K4 and L4. The third class is illustrated by J2, J3, K3, and L3 both with the height of the upper section $h \approx L_0$ and results in lamellae completely parallel to both of the top and bottom surfaces. In addition, some hybrid complex structures appear in Figure 3, such as K2.

As pointed out by Geisinger et al.,[42] for neutral walls, the lamellae perpendicular to the substrates were always stable in confined films. The confinement films can reduce the chain configuration entropy by either compressing or stretching the chains. Thus, the first class morphologies with lamellae parallel to the top surface and perpendicular to the bottom surface are expected. In fact, these structures occupy most of the phase areas in Figure 3. In contrast to the ideal symmetric confined surfaces, however, there are some particularities of the A/B interfaces because of the connectivity of the two parts in this confined geometry. For relatively small upper section width $w/L_0 = 0.43$ (i.e., almost half of bulk lamellae period L_0), we illustrate the particularities of the A/B interfaces cited as $D/L_0 = 0.96$ (i.e., almost one bulk lamellae period L_0). Parallel lamellae with one A/B interface ($v = 1$) are formed in the upper section, and the

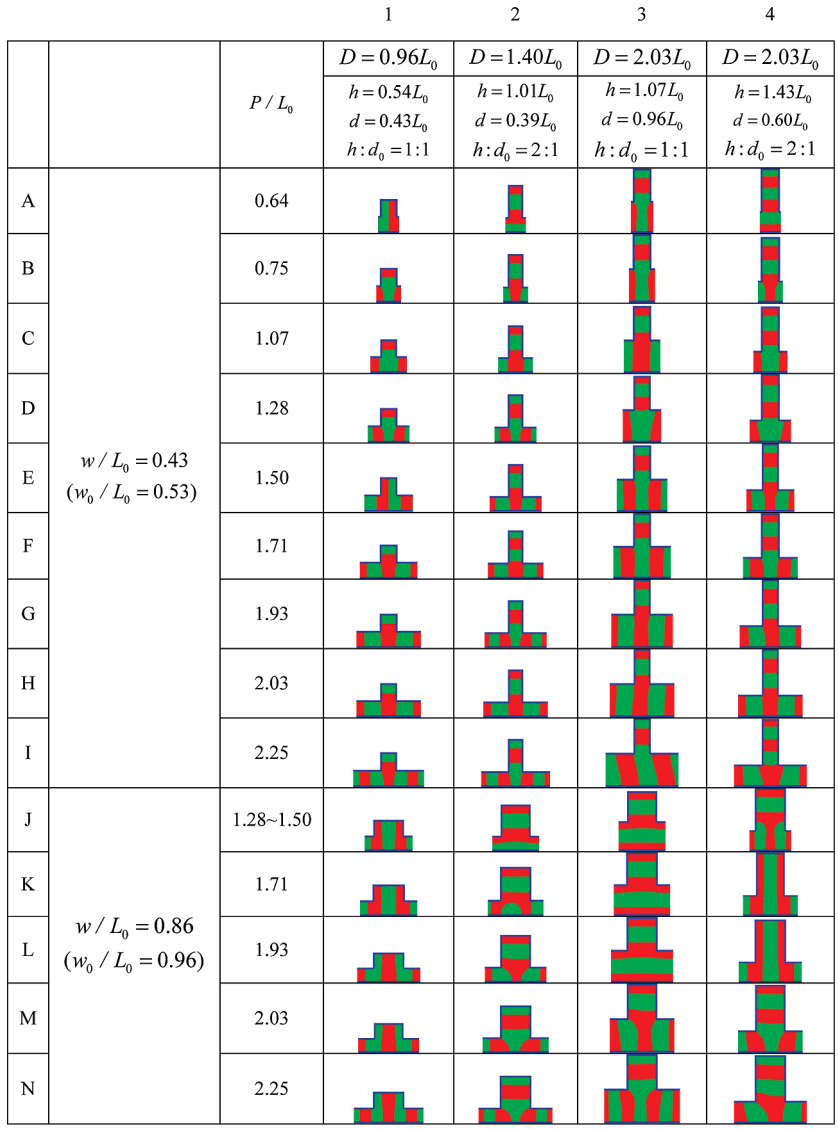

Figure 3. Representative microstructures of symmetric confined diblock copolymers with $f_A = 0.5$ and $\chi_{AB}N = 35$ for the case of neutral walls $\chi_{AW}N = \chi_{BW}N = 0$ with various confinement sizes including w/L_0, D/L_0, h/L_0, d/L_0, and P/L_0. The red and green colors represent the A and B blocks, respectively.

number of interfaces of lamellae υ in the lower section is influenced by the period of the square wave P. In particular, when P is not commensurate with L_0, the usual flat A/B interfaces are curved to some degree, forming arcs at the corners of the joining regions, as shown in B1, D1, F1, and I1; A/B interfaces become flat when P is almost equal to the integer period L_0, as shown in C1 and H1. Similar phenomena are found at almost all thicknesses D (columns 1−4) and $w/L_0 = 0.43$. It is interesting that, for relatively wide upper sections such as $w/L_0 = 0.86$, the curved A/B interface occurs when P is commensurate with L_0, as shown in L2, M2, N2, M3, N3, J4, M4, and N4. The occurrence of curved A/B interfaces provides a convenient transition between the parallel lamellae in the upper section and the perpendicular lamellae in the lower section. It should be noted that the perpendicular lamellae in the lower section of structure I3 slant slightly, because P is slightly larger than $2L_0$, and the thickness of the lower section d_0 is equal to L_0, allowing the perpendicular lamellae to wave slightly. Moreover, whether P is commensurate with L_0 or not, the value of P can modulate the number of A/B interfaces in the convex confinement thickness D, such as from E2 ($\upsilon = 2$) to F2 ($\upsilon = 3$) to G2 ($\upsilon = 2$) to H2 ($\upsilon = 2$) to H4 ($\upsilon = 3$) and to I4 ($\upsilon = 4$). In addition, when P does not match the bulk lamella period L_0, some special structures such as completely perpendicular lamellae A1, E1 and completely parallel lamellae A2, A4 are obtained due to the competition effects between A/B interaction energy and confinement of the geometrical structures. For instance, the incommensuration of the period of the square wave P with L_0 leads to lamellae in the upper section aligned perpendicular to the top surface, forming completely perpendicular lamellae, as shown in A1 and E1 in Figure 3. The perpendicular lamellae were also shown by He et al.[54] when the thickness of the lower section was relatively small. Similarly, completely parallel lamellae occur, as shown in A2 and A4 in Figure 3. We should note that the reason for the formation of completely perpendicular lamellae A1, E1 and completely parallel lamellae A2, A4 is different from the second and third class of structures, as discussed below. Figure 4 displays the free energy of the system as a function of P/L_0. Evidently, A1 and E1 have much higher free energy, as shown in curve I ($w/L_0 = 0.43$), and the free energy reaches a minimum when the period of the square wave P is an integer multiple of the bulk repeat period L_0. Subsequently, the value of F/nK_bT increases as the number of A/B interfaces υ in the lower section is changed

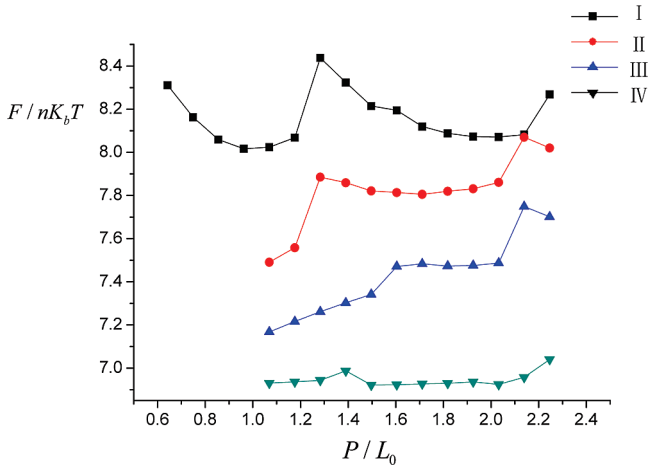

Figure 4. Free energy as predicted by SCFT theory as a function of width of the lower section P/L_0 along the x direction. I: $w/L_0 = 0.43$, $D/L_0 = 0.96$, and $h/d_0 = 1{:}1$ ($h = 0.54L_0$, $d = 0.43L_0$). II: $w/L_0 = 0.86$, $D/L_0 = 0.96$, and $h/d_0 = 1{:}1$ ($h = 0.54L_0$, $d = 0.43L_0$). III: $w/L_0 = 0.86$, $D/L_0 = 1.40$, and $h/d_0 = 2{:}1$ ($h = 1.01L_0$, $d = 0.39L_0$). IV: $w/L_0 = 0.86$, $D/L_0 = 2.03$, and $h/d_0 = 1{:}1$ ($h = 1.07L_0$, $d = 0.96L_0$). The corresponding morphologies are shown in Figure 3.

from $v = 2$ to $v = 4$ and then decreases until $P \approx 2L_0$. Therefore, P determines the confined geometrical shape, which has a significant influence on the structures of block copolymers.

The second class structures, namely, lamellae completely aligned perpendicular to both of the top and bottom surfaces for the case of $w/L_0 = 0.86$, $D/L_0 = 0.96$, $h \approx d \approx 0.5L_0$ (i.e., $w \approx L_0$ and $h < w$) and K4, L4, as shown in Figure 3, are found to be stable due to the suitable width w of the upper section and uncomfortable lower section thickness d and height of upper section h. When the width of the upper section w is about one lamellae bulk period L_0, perpendicular lamellae are found to be stable. Furthermore, perpendicular lamellae confined in the lower section perfectly joined to those in the upper section will result in more stable microstructures in the confinement geometry. From the free energy of the system in Figure 4, curve II, comparing with curve I, when the period of the square wave P is an integer multiple of the polymer bulk period L_0, the free energy reaches minimum and is almost constant between $P = 1.2L_0$ and $P = 2L_0$, indicating that the perpendicular lamellae of curve II are more stable than those of curve I as a function of P. Especially when both h and d are not commensurate with the bulk lamellae period L_0 of the diblock copolymer (i.e., column 4 with $w/L_0 = 0.86$), P plays a critical role in directing the lamellae alignment transition between parallel and perpendicular lamellae in order to satisfy the confining boundaries.

When both of the height of the upper section h and lower section thickness d are commensurate with the bulk lamella period L_0 (i.e., $h = d \approx L_0$), the completely parallel lamellae J3, K3, and L3 appear with the lowest and most stable free energy as a function of the period of the square wave P (see Figure 4, curve IV), which is similar to the experimental results by Kim et al.[39] As P increases to $2.03L_0$, confinement of the geometrical structures no longer plays a leading role so that the copolymers acquire freedom to form perpendicular lamellae in the lower section such as M3. Subsequently, when P increases to $2.25L_0$ in N3, the number of the A/B interfaces in the lower section increases from $v = 4$ to $v = 6$, and the value of F/nK_bT of N3 is a little larger than that of M3 (see Figure 4, curve IV). For neutral parallel walls, the parallel lamellar morphology has identical free energy to that of perpendicular lamellae only if the film thickness coincides with half integer multiples of the bulk period.[42] The appearance of parallel lamellae in J2 at $h = L_0$ and $d \approx 0.5L_0$ is thus expected. However, as P increases to $1.71L_0$, the hybrid complex structure K2 occurs, as it requires too much energy of the system to form parallel lamellae in the lower section (see Figure 4, curve III). In fact, K2 is the transition structure from parallel (J2) to perpendicular (L2) lamellae in the lower section. In our explored parameter space, the hybrid complex structure only occurs in K2 for the case of $w = h = L_0$, $d = 0.5L_0$, and $P = 1.60-1.71L_0$.

B. Strong A-Repellent Walls. We now consider the effect of the surface field on the microstructure of the confined symmetric AB diblock copolymers. We evaluate two situations corresponding to relatively strongly repulsive ($\chi_{AW}N = 20$) and weakly repulsive ($\chi_{AW}N = 10$) surfaces for the A block, respectively. In this section, we first explore morphologies for strongly repulsive ($\chi_{AW}N = 20$) surfaces, shown in Figure 5. In this case, the A block is strongly repelled away from the walls, mostly leading to the preference of the B block to the surfaces. From Figure 5, the most commonly observed structures are the completely parallel lamellae found in column 1 for all confined sizes from $w/L_0 = 0.43$ to $w/L_0 = 2.35$ or from column 1 to column 6 with $w/L_0 = 0.43$, i.e., w or height of upper section h is relatively small. The structure with parallel lamellae in the upper section and the perpendicular lamellae in the lower section, i.e., the first class structure shown in Figure 3, only occurs in B1. Some additional new structures occur in comparison with Figure 3. For instance, the inverted T-style structures with perpendicular lamellae in the upper section along with parallel lamellae in the lower section are found, as shown from column 2 to column 6 with the width size $w/L_0 = 0.86$, which was also found in Kim's experimental work.[39] Furthermore, special structures, such as square or partial square structures in the upper section and parallel lamellae in the lower section, occur in columns 5 and 6 with relatively large values of $w/L_0 = 1.39$, $w/L_0 = 1.82$, and $w/L_0 = 2.35$, i.e., $h \geq 1.36L_0$ and $w \geq 1.39L_0$.

Previous work[18,42] revealed that preferential walls toward one of the polymer species resulted in lamellae aligned with the film producing a parallel lamellar phase. Ideally, the number of A/B interfaces v in the film equals $2D/L_0$, allowing the lamellae to acquire their preferred thickness. Therefore, when the convex film thickness D is an integer multiple of L_0, such as $D/L_0 = 0.96$, $D/L_0 = 1.93$, and $h{:}d = 1{:}1$, parallel lamellae with even integers v in the convex film thicknesses D are found. Although in column 2 the thickness $D = 1.40L_0$ is not commensurate with L_0, parallel lamellae also exist due to the comfortable height of upper section h. However, this structure cannot stably exist in the case of parallel surface confinement. At the lower section of the confinement, the A blocks are connected to the upper surfaces of the lower section (see in columns 1, 2, and 4) due to the relatively small lower section d and the odd-integer number of A/B interfaces, which was also obtained in Turner's work.[7] For relatively small $w/L_0 = 0.43$, the confinement effect becomes more important and tends to form parallel lamellae in the upper section, i.e., perpendicular to the vertical surfaces. In particular, the structure with the parallel lamellae in the upper section and the perpendicular lamellae in the lower section only occurs in B1 with $P \approx L_0$ in our explored parameter space for the relatively strong surface field ($\chi_{AW}N = 20$). However, with increasing period of the square wave P, perpendicular lamellae emerge at the edges of the lower section, as shown in G2, J2, and N2. The similar phenomenon called "perforation" by Podariu et al.[31] were well-known, and the number of perforations was increased as the

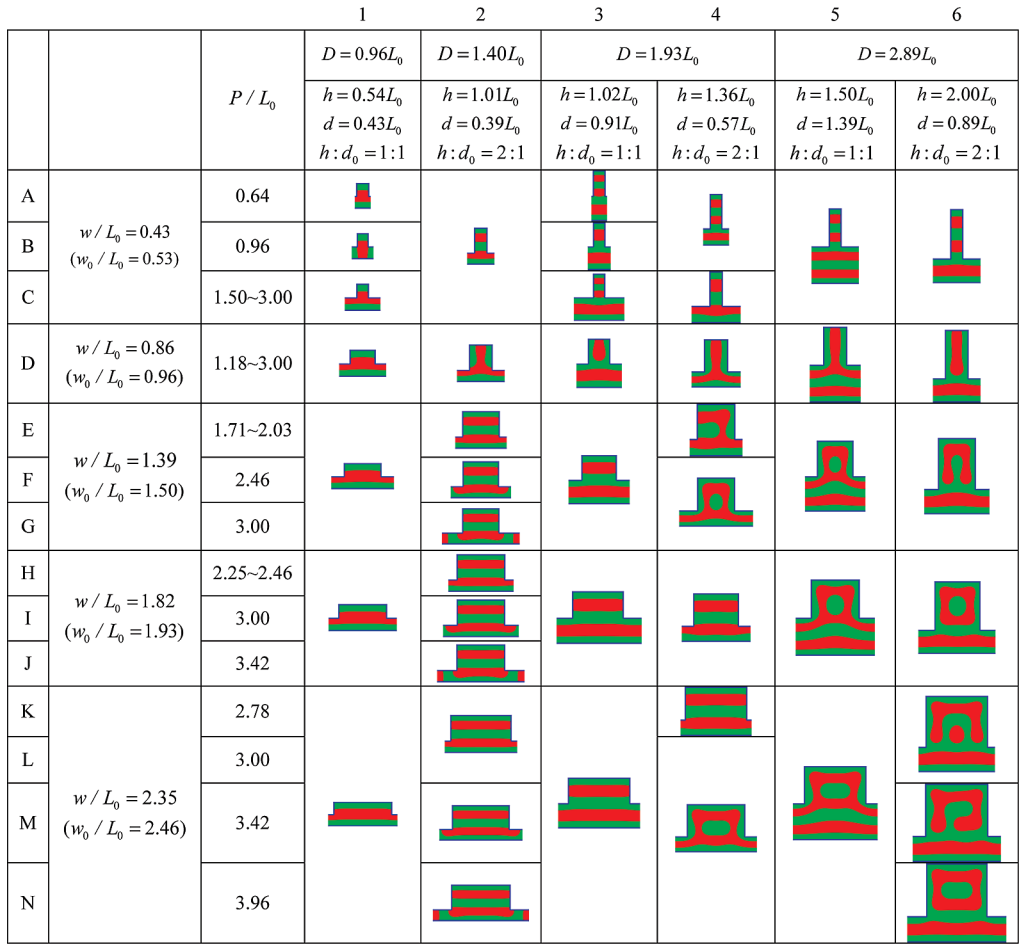

Figure 5. Representative microstructures of the symmetric confined diblock copolymer $\chi_{AB}N = 35$ for the strong A-repellent walls $\chi_{AW}N = 20$, $\chi_{BW}N = 0$ with various confinement sizes: w/L_0, D/L_0, h/L_0, d/L_0, and P/L_0. The red and green colors represent the A and B blocks, respectively.

surface field was increased. In fact, such a perpendicular structure was also widely found in cylinder-forming asymmetric diblock[17] and star ABC triblock copolymers under confinement.[56] We conclude that this kind of topography can easily induce the formation of parallel lamellae, even if the copolymers are confined in uncomfortable thicknesses, rather than perpendicular lamellae which cost too much elastic energy to wet the surfaces.[53] In general, when the upper section width w is relatively small (i.e.,$w/L_0 = 0.43$) or w is larger than the height of the upper section h such as D−N in column 1 and E−N in column 3, completely parallel lamellae are always stable.

Perpendicular lamella structures in the upper section appear at $w/L_0 = 0.86$ from column 2 to column 6. Furthermore, when the height of the upper section h and the thickness of the lower section d have integer numbers of the bulk lamella period L_0, i.e., $h = d \approx 1L_0$ (column 3) and $h \approx 2L_0$, $d \approx 1L_0$ (column 6), the repulsive A blocks are not connected to the lower section. In contrast, for the case of $h = 1.36L_0$, $d = 0.57L_0$ (column 4), and $h \approx d \approx 1.5L_0$ (column 5), the A blocks are joined together, forming inverted T-style structures, following our confined geometrical shape. The number of A/B interfaces in the lower section increases by enhancing the convex film thickness D and the lower section thickness d. Square or partial square structures in the upper section combined with the parallel lamellae in the lower section appear in columns 5 and 6 at relatively large width w and height h of the upper section, i.e., $w \geq 1.39L_0$ and $h \geq 1.36L_0$. Whether copolymers form square structures (H6, I6, J6, and N6) or partial square structures (E6, F6, G6, K6, L6, and M6) or whether copolymers form square structures connected to the lower section (in column 5 from E to N, F4, G4, L4, M4, and N4), all thicknesses of the films D, h, d, w, and P can induce the copolymers to acquire their preferred microstructures. It is noted that these results are largely unchanged for even stronger interactions between copolymer A and the surfaces such as $\chi_{AW}N = 40$ (not shown here).

C. Weak A-Repellent Walls. Figure 6 presents the morphology of confined AB diblock copolymers for a weak surface field at $\chi_{AW}N = 10$. In comparison to $\chi_{AW}N = 20$, the structures are similar to those in Figure 5 at relatively large thickness $D = 1.93L_0$ (h:d_0 = 1:1) and $D = 2.89L_0$ (h:d_0 = 1:1) for the upper section widths from $w/L_0 = 0.43$ to $w/L_0 = 2.35$. However, we observe some different structures at relatively small thickness such as $D = 0.96L_0$ (h:d_0 = 1:1) in all confined widths in the upper section from $w/L_0 = 0.43$ to $w/L_0 = 2.35$, and the relatively large thickness $D = 2.89L_0$ (h:d_0 = 2:1) with $w/L_0 = 1.82$ and $w/L_0 = 2.35$. From Figure 6, perpendicular lamellae in the lower section exist at small thicknesses $D = 0.96L_0$ in diagrams 1−5 and $D = 1.40L_0$ in diagrams 1 and 2. In this case, the geometric confinement dominates rather than the weak surface field in determining the phase structure. The perpendicular lamellae in relatively weak surface field were also found in Poduriu's work.[31] As Matsen[15,18] pointed out, frustration in the parallel lamellae phase could be relieved if the parallel lamellae flip, forming lamellae perpendicular to the film. Although such a phase has unfavorable surface energy, its period is free to relax to the bulk lamella period L_0. When the period

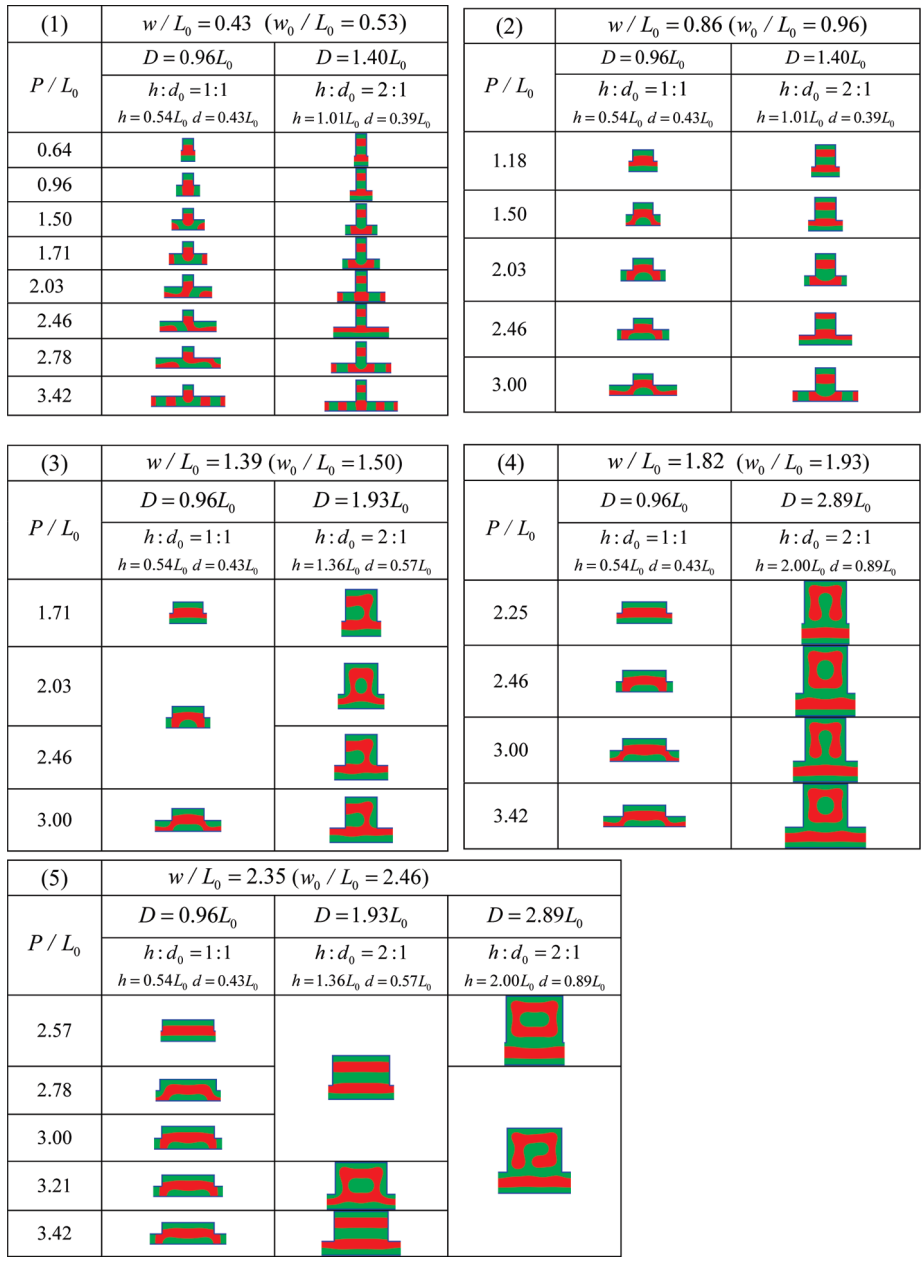

Figure 6. Microstructures of confined symmetric diblock copolymer $\chi_{AB}N = 35$ for the weak A-repellent walls $\chi_{AW}N = 10$, $\chi_{BW}N = 0$ compared to the strong A-repellent walls shown in Figure 5 with various confinement sizes: w/L_0, D/L_0, h/L_0, d/L_0, and P/L_0.

of the square wave P increases to $3L_0$, parallel lamellae occurring in the lower section are obtained again, as shown in diagrams 2−5. The translation from parallel to perpendicular lamellar layers on corrugated surfaces as a function of the depth of the confinement and the period of corrugated surface pattern was also reported by Tsori et al.[32] In addition, as shown in diagrams 2−5, when $w \geq L_0$, relatively thin convex thickness $D = 0.96L_0$ and $P \geq 3L_0$, the parallel lamellae in the upper and lower sections are connected at the corner, forming trapezoid structures, in which the repellent A domains almost imitate the shape of the square-wave top surface. With increasing width of the upper section w and convex film thickness D (such as $D = 1.93L_0$ shown in diagrams 3 and 5 and $D = 2.89L_0$ shown in diagram 4), the square or partial square structures in the upper section combined with parallel lamellae in the lower section appear as a function of P, but the translations between the square and partial square structures with increasing P are more common than the case of strong surface field shown in Figure 4. This behavior is attributed to the intense interplay between the relatively weak surface field and the variation of geometrical confinement structures. In addition, some hybrid complex structures in diagram 1 with $D = 0.96L_0$ reported by previous works[18,54] mainly originate from the competition between surface−copolymer interaction energy and confinement geometry.

We should note that in this work the film model with flat lower surface and the square-wave upper surface is analogous to the experimental report by Kim et al.[39] Although we have obtained some structures such as the completely parallel lamellae for both of the neutral walls and A-repellent walls and the reversed-T structures for strong A-repellent walls, the comparison of the simulation results with the experimental results is not direct or quantitative because of the different aspect ratio of confined geometry. In Kim's experiments, the convex thickness $D_0(D)$ of the film is about 28−30 lamellae periods of bulk block copolymers L_0 and the height of the upper section h is about $22L_0$, which are much larger than those in our

simulations (the convex thickness $D_0(D)$ is about $(1-3)L_0$ and h is about $(0.5-2)L_0$). Due to the limitation of real-space implementation of the SCFT equations, it is not suitable to deal with relatively large computation size; i.e., the computation size is available only for several periods of bulk block copolymers. However, for periodical structures, obtaining the structure characteristics is just our focus. Furthermore, we also do simulations for relatively large system size and the phase behavior is similar to that in bulk. In other words, only relatively small confinement size can emphasize the confined geometry effect on the phase behavior. Furthermore, in the recent experimental study,[40] perpendicular lamellae were found when the thickness of the films was double the depth of the film upper section, which are very similar to the structures J1, K1, L1, M1, and N1 shown in Figure 3. We both found that the alignment of lamellae is strongly dependent on the relative film thickness to corrugation depth as well as the period of the surface corrugation pattern. In the experimental work,[30] when the substrate features were of such height that film thickness modulates about $L_0/2$, the film domains decorated the peaks of the corrugated substrate, forming a patterned film that reflected the topography beneath. This phenomenon is very similar to the trapezoid structures formed in the relatively weak surface field in our work, which also follow the square-wave topographically patterned surface.

Conclusions

We have described the ordered phase behavior of symmetric AB diblock copolymers confined between two horizontal asymmetrical topographical surfaces, of which the lower surface is flat and the upper surface is a square wave. By embedding the irregularly shaped domains into a larger rectangular box with the help of the so-called "masking" hyperbolic tangent functional form, an efficient and high-order accurate pseudospectral method involving fast Fourier transform is adopted to numerically solve the SCFT equations in the rectangular box subjected to periodic boundary conditions. In principle, this technique can deal with any irregular geometric shape under confinement provided that the confined boundary is designed with suitable hyperbolic tangent functions. The phase structure of AB diblock copolymer thin films in this work is systematically tuned with the variation of geometrical shape parameters of the confining template, including the convex thicknesses D, the thickness of the lower section d, the width of the upper section w, the height of the upper section h, and the period of the square wave P and the surface field.

In our study, the inverted T-style and trapezoid structures almost imitate the confined geometrical shape. The inverted T-style structures are formed in the relatively strong surface field when the width of the upper section w is nearly equal to the bulk lamella period L_0 and the height of the upper section $h \geq L_0$. The trapezoid structures are formed in the relatively weak surface field when $w \geq L_0$, relatively thin convex thickness $D = 0.96L_0$, and the period of the square wave P is large enough. For the case of neutral walls, completely perpendicular lamellae emerge when the width of the upper section is commensurate with L_0 (i.e., $w \approx L_0$ and $h < w$), and completely parallel lamellae are favored when both the width and height of the upper section are equal to L_0. Furthermore, in the neutral surface field, the most prevalent structures are arrangement of parallel lamellae in the upper section combined with perpendicular lamellae in the lower section when w is relatively small and $w \leq h$, since the confinement geometrical structures dominate the phase morphologies. When the walls repel relatively strongly one of the block species, parallel lamellae are stably induced by the topographical surfaces in a wide range of film geometries, thus reducing the complex phases. When the width w and the height h of the upper section are large enough, i.e., $h \geq 1.36L_0$ and $w \geq 1.39L_0$, square and partial square structures in the upper section of the confinement are obtained. For relatively weak surface fields, both confinement geometrical structures and the surface fields play critical roles in controlling the phase behavior. Therefore, increasing the period of the square wave P, much more complicated structures are found with different parameters D, d, w, and h, such as the parallel lamellae in the upper section combined with perpendicular lamellae in the lower section, trapezoid structures, square and partial square structures, and so on. In general, the required phase structures can be obtained by choosing proper parameters of the confined template and surface field. Moreover, the period of the square wave P plays a critical role in controlling the phase behavior. Our simulation results provide a guide to understanding the complex interplay between confinement effects and surface field in the morphology performance of nanoimprinted symmetric diblock copolymers.

Acknowledgment. We appreciate the financial support from the National Basic Research Program of China (Grant No. 2005CB623800). Funds from the NSF of China (Grant Nos. 20474012, 20674012) and Senior Visiting Scholar Foundation of Key Laboratory in Fudan University are also acknowledged.

References and Notes

(1) Bates, F. S.; Fredrickson, G. H. *Annu. Rev. Phys. Chem.* **1990**, *41*, 525.
(2) Bates, F. S.; Fredrickson, G. H. *Phys. Today* **1999**, *52*, 32.
(3) Matsen, M. W. *J. Phys.: Condens. Matter* **2002**, *14*, R21.
(4) Park, M.; Harrison, C.; Chaikin, P. M.; Register, R. A.; Adamson, D. H. *Science* **1997**, *276*, 1401.
(5) Segalman, R. A. *Mater. Sci. Eng., R* **2005**, *48*, 191.
(6) Lambooy, P.; Russell, T. P.; Kellogg, G. J.; Mayes, A. M.; Gallagher, P. D.; Satija, S. K. *Phys. Rev. Lett.* **1994**, *72*, 2899.
(7) Turner, M. S. *Phys. Rev. Lett.* **1992**, *69*, 1788.
(8) Turner, M. S.; Rubinstein, M.; Marques, C. M. *Macromolecules* **1994**, *27*, 4986.
(9) Cheng, J. Y.; Ross, C. A.; Thomas, E. L.; Smith, H. I.; Vancso, G. J. *Appl. Phys. Lett.* **2002**, *81*, 3657.
(10) Segalman, R. A.; Yokoyama, H.; Kramer, E. J. *Adv. Mater.* **2001**, *13*, 1152.
(11) Ruiz, R.; Kang, H. M.; Detcheverry, F. A.; Dobisz, E.; Kercher, D. S.; Albrecht, T. R.; de Pablo, J. J.; Nealey, P. F. *Science* **2008**, *321*, 936.
(12) Bita, I.; Yang, J. K. W.; Jung, Y. S.; Ross, C. A.; Thomas, E. L.; Berggren, K. K. *Science* **2008**, *321*, 939.
(13) Tang, C. B.; Lennon, E. M.; Fredrickson, G. H.; Kramer, E. J.; Hawker, C. J. *Science* **2008**, *322*, 429.
(14) Walton, D. G.; Kellogg, G. J.; Mayes, A. M.; Lambooy, P.; Russell, T. P. *Macromolecules* **1994**, *27*, 6225.
(15) Kellogg, G. J.; Walton, D. G.; Mayes, A. M.; Lambooy, P.; Russell, T. P.; Gallagher, P. D.; Satija, S. K. *Phys. Rev. Lett.* **1996**, *76*, 2503.
(16) Kellogg, G. J.; Walton, D. G.; Mayes, A. M.; Lambooy, P.; Russell, T. P.; Gallagher, P. D.; Satija, S. K. *Phys. Rev. Lett.* **1996**, *76*, 2503.
(17) Yang, Y. Z.; Qiu, F.; Zhang, H. D.; Yang, Y. L. *Polymer* **2006**, *47*, 2205.
(18) Matsen, M. W. *J. Chem. Phys.* **1997**, *106*, 7781.
(19) Wang, Q.; Yan, Q. L.; Nealey, P. F.; de Pablo, J. J. *J. Chem. Phys.* **2000**, *112*, 450.
(20) Huinink, H. P.; Brokken-Zijp, J. C. M.; van Dijk, M. A.; Sevink, G. J. A. *J. Chem. Phys.* **2000**, *112*, 2452.
(21) Wang, Q.; Nealey, P. F.; de Pablo, J. J. *Macromolecules* **2001**, *34*, 3458.
(22) Heckmann, M.; Drossel, B. *Macromolecules* **2008**, *41*, 7679.
(23) Niihara, K. I.; Sugimori, H.; Matsuwaki, U.; Hirato, F.; Morita, H.; Doi, M.; Masunaga, H.; Sasaki, S.; Jinnai, H. *Macromolecules* **2008**, *41*, 9318.
(24) Sevink, G. J. A.; Zvelindovsky, A. V.; Fraaije, J.; Huinink, H. P. *J. Chem. Phys.* **2001**, *115*, 8226.
(25) Li, W. H.; Wickham, R. A.; Garbary, R. A. *Macromolecules* **2006**, *39*, 806.

(26) Yu, B.; Sun, P. C.; Chen, T. H.; Jin, Q. H.; Ding, D. T.; Li, B. H.; Shi, A. C. *J. Chem. Phys.* **2007**, *127*, 15.
(27) Bosse, A. W.; Garcia-Cervera, C. J.; Fredrickson, G. H. *Macromolecules* **2007**, *40*, 9570.
(28) He, X. H.; Song, M.; Liang, H. J.; Pan, C. Y. *J. Chem. Phys.* **2001**, *114*, 10510.
(29) Chen, P.; Liang, H. J.; Shi, A. C. *Macromolecules* **2008**, *41*, 8938.
(30) Fasolka, M. J.; Harris, D. J.; Mayes, A. M.; Yoon, M.; Mochrie, S. G. J. *Phys. Rev. Lett.* **1997**, *79*, 3018.
(31) Podariu, I.; Chakrabarti, A. *J. Chem. Phys.* **2000**, *113*, 6423.
(32) Tsori, Y.; Andelman, D. *Macromolecules* **2003**, *36*, 8560.
(33) Lee, J. Y.; Shou, Z. Y.; Balazs, A. C. *Macromolecules* **2003**, *36*, 7730.
(34) He, L. L.; Zhang, L. X.; Liang, H. J. *Polymer* **2009**, *50*, 721.
(35) Shin, D. O.; Kim, B. H.; Kang, J. H.; Jeong, S. J.; Park, S. H.; Lee, Y. H.; Kim, S. O. *Macromolecules* **2009**, *42*, 1189.
(36) Tada, Y.; Akasaka, S.; Yoshida, H.; Hasegawa, H.; Dobisz, E.; Kercher, D.; Takenaka, M. *Macromolecules* **2008**, *41*, 9267.
(37) Cheng, J. Y.; Rettner, C. T.; Sanders, D. P.; Kim, H. C.; Hinsberg, W. D. *Adv. Mater.* **2008**, *20*, 3155.
(38) Segalman, R. A. *Science* **2008**, *321*, 919.
(39) Kim, S.; Lee, J.; Jeon, S. M.; Lee, H. H.; Char, K.; Sohn, B. H. *Macromolecules* **2008**, *41*, 3401.
(40) Park, S. M.; Berry, B. C.; Dobisz, E.; Kim, H. C. *Soft Matter* **2009**, *5*, 957.
(41) Kikuchi, M.; Binder, K. *J. Chem. Phys.* **1994**, *101*, 3367.
(42) Geisinger, T.; Muller, M.; Binder, K. *J. Chem. Phys.* **1999**, *111*, 5241.
(43) Geisinger, T.; Muller, M.; Binder, K. *J. Chem. Phys.* **1999**, *111*, 5251.
(44) Frischknecht, A. L.; Curro, J. G.; Frink, L. J. D. *J. Chem. Phys.* **2002**, *117*, 10398.
(45) Shull, K. R. *Macromolecules* **1992**, *25*, 2122.
(46) Kikuchi, M.; Binder, K. *Europhys. Lett.* **1993**, *21*, 427.
(47) Milner, S. T.; Morse, D. C. *Phys. Rev. E* **1996**, *54*, 3793.
(48) Fasolka, M. J.; Banerjee, P.; Mayes, A. M.; Pickett, G.; Balazs, A. C. *Macromolecules* **2000**, *33*, 5702.
(49) Drolet, F.; Fredrickson, G. H. *Phys. Rev. Lett.* **1999**, *83*, 4317.
(50) Drolet, F.; Fredrickson, G. H. *Macromolecules* **2001**, *34*, 5317.
(51) Helfand, E. *J. Chem. Phys.* **1975**, *62*, 999.
(52) Meng, D.; Wang, Q. *J. Chem. Phys.* **2007**, *126*, 234902.
(53) Khanna, V.; Cochran, E. W.; Hexemer, A.; Stein, G. E.; Fredrickson, G. H.; Kramer, E. J.; Li, X.; Wang, J.; Hahn, S. F. *Macromolecules* **2006**, *39*, 9346.
(54) He, L. L.; Zhang, L. X.; Liang, H. J. *J. Polym. Sci., Part B: Polym. Phys.* **2009**, *47*, 1.
(55) Tzeremes, G.; Rasmussen, K. O.; Lookman, T.; Saxena, A. *Phys. Rev. E* **2002**, *65*, 5.
(56) Han, W. C.; Tang, P.; Li, X.; Qiu, F.; Zhang, H. D.; Yang, Y. L. *J. Phys. Chem. B* **2008**, *112*, 13738.

JP9033613